geosciences

MDPI

Article

Estimation of Radon Flux Density Changes in Temporal Vicinity of the Shipunskoe Earthquake with $M_w = 7.0$, 17 August 2024 with the Use of the Hereditary Mathematical Model

Dmitrii Tverdyi [1], Evgeny Makarov [2] and Roman Parovik [1,*]

[1] Institute of Cosmophysical Research and Radio Wave Propagation FEB RAS, Paratunka, Mirnaya Street 7, 684034 Kamchatka, Russia; tverdyi@ikir.ru
[2] Kamchatka Branch of the Federal Research Center "Unified Geophysical Service of the Russian Academy of Sciences", Petropavlovsk-Kamchatsky, Piipa Boulevard St. 9, 683023 Kamchatka, Russia; ice@emsd.ru
* Correspondence: parovik@ikir.ru

Abstract: Using the data of radon accumulation in a chamber with excess volume at one of the points of the Kamchatka subsurface gas-monitoring network, the change in radon flux density due to seismic waves and post-seismic relaxation of the medium is shown. A linear fractional equation is considered to be a model equation. The change of radon-transport intensity due to changes in the state of the geo-environment is described by a fractional Gerasimov–Caputo derivative of constant order. Presumably, the order of the fractional derivative is related to the radon-transport intensity in the geosphere. Using the Levenberg–Marquardt method, the optimal values of the model parameters were determined based on experimental data: air exchange coefficient and order of fractional derivative, which allowed the solving of the problems of radon flux density determination. Data in the temporal neighborhood of a strong earthquake with $M_w = 7.0$, which occurred in the northern part of Avacha Bay on 17 August 2024, were used. As a result of the modeling, it is shown that the strong seismic impact and subsequent processes led to changes in the radon flux in the accumulation chamber. The obtained model curves agree well with the real data, and the obtained estimates of radon flux density agree with the theory.

Keywords: mathematical modeling; radon volumetric activity; radon flux density; earthquake precursors; Gerasimov–Caputo fractional derivative; memory effect; non-locality; inverse problems; Levenberg–Marquardt algorithm; MATLAB; C; Gnuplot

MSC: 26A33; 86A22; 49N45

Academic Editor: Dimitrios Nikolopoulos

Received: 30 November 2024
Revised: 9 January 2025
Accepted: 14 January 2025
Published: 16 January 2025

Citation: Tverdyi, D.; Makarov, E.; Parovik, R. Estimation of Radon Flux Density Changes in Temporal Vicinity of the Shipunskoe Earthquake with $M_w = 7.0$, 17 August 2024 with the Use of the Hereditary Mathematical Model. *Geosciences* **2025**, *15*, 30. https://doi.org/10.3390/geosciences15010030

1. Introduction

Throughout the geologic history of Earth, water–gas fluid flows have been continuously emitted from its interior, which vary markedly in time and are unevenly distributed on the surface of our planet, reflecting its geodynamic regime, block structure, and placement of fault zones [1,2]. At present, geophysics has developed the idea of geological medium as a hierarchically self-similar open non-equilibrium system of separates, in which the seismic process is a consequence of the deformation of the medium under the action of tectonic forces. The potential energy accumulated in the structural volumes of such medium during its deformation is dissipated mainly on the systems of faults and blocks of different scale levels. As modern experimental and theoretical studies have shown, the diagnosis of criticality level and prediction of catastrophic earthquakes should be based,

first, on the existing interaction between global and local geomechanical fields in the upper part of Earth's crust of block-hierarchical structure.

The recorded character and peculiarities of the response of the medium to earthquake preparation depend on the type of observations, the type of equipment used, and the strain sensitivity of the observation point. Works on investigation of the connection of radon gas dynamics (^{222}Rn) with seismicity are carried out in many countries located in seismically active areas of the world (Israel, India, Japan, USA, China, Russia). The precursor anomalies are sought in the dynamics of subsurface radon, radon in atmospheric air, and dissolved radon in thermal waters. Examples of such precursor anomalies have been published in numerous articles, a review of which can be found in the works of [3–8], where numerous data on radon precursors are collected and systematized. The paper [9] is the most relevant and contains a large literature review of electromagnetic and radon precursors for earthquakes. This work also details mathematical methods for analyzing data from electromagnetic radiation and radon concentration measurements and explores physical models of earthquake occurrence to interpret the causes of precursors [9].

As a rule, the literature considers the amplitude of the anomaly, the lead time to the moment of seismic event occurrence, and the duration of the anomaly. In almost all works devoted to radon precursors, their selection is based on the temporal confinement to strong earthquakes relative to the background, as a rule, in one point [10–15]. Due to the rapid progress of observational tools, automatic stations are now being used to comprehensively record the gas composition of subsurface air [16]. In this case, anomalies are highlighted with greater certainty. The lead times of radon earthquake precursors range from hours to several years, i.e., both short-term and long-term precursors are observed. Therefore, the occurrence of precursors with such a time range of anticipation is clearly due to various geodynamic processes that require their own study. The amplitude of anomalies is most often within 20–200% of the background, but cases of exceeding by more than 1200% have been noted. It should be noted that negative anomalies were also observed among radon precursors.

The prospect of the radon method for the purpose of monitoring geodynamic processes, in particular, predicting earthquakes and mountain shocks, has been shown in numerous works, references to which can be found in reviews [4–6,9,17]. These works describe various possible mechanisms of radon anomalies related to changes in fracturing and permeability of the medium, changes in fluid flow, etc. Work is underway to monitor subsurface gas concentrations in order to predict volcanic eruptions [18,19]. A number of review papers, where numerous data on radon precursors have been collected and systematized, describe anomalies with lead times ranging from hours to several years. Thus, in the work of more than 30 years old [3] based on data for a ten-year observation period in the territory of China, 4 types of radon precursors with different lead times were identified: long-term (several years), medium-term (about a year), short-term (2–6 months), and operational (hours to days). In the paper [4], the analysis of 83 known at that time radon precursors registered in different seismically active regions of the world by the end of the 80s of the last century was made: 28 in Central Asia on the territory of the USSR, 15 in China, 4 in the Caucasus, 32 in North America (USA). Attention was paid to their temporal forms, and empirical relationships were found between the parameters of precursor anomalies (amplitude, preemptive time) and earthquake parameters (magnitude, distance). In a review work done ten years later [5], attention is drawn to the peculiarities of radon anomalies, and an attempt is made to explain their physical nature. The work, written about a quarter of a century ago, and today has not lost its relevance. It notes that radon precursors have a great variety of forms of different duration and are registered at considerable distances from the epicenters of both shallow and deep earthquakes with a

range of magnitudes $M_w = 4 - 8$. In the opinion of the author of [5], the observed anomalies ^{222}Rn may occur at small deformations associated with changes in the stress-strain state of the geosphere at the point of observation. In the paper [6], the analysis of radon precursors is carried out on a wider material, data on 125 precursors in the radon field before 86 earthquakes with $M_w = 2.5 - 8$ are given. Most observations were made before earthquakes with $M_w > 4$.

Modern researchers continue to consider issues related to the influence of deformation processes on radon migration in rocks and various materials [20–22]. In [23], it is shown that at triaxial compression of rock salt formation, the emanation of geogenic noble gases correlates with volumetric strain and acoustic emission. At low pressures, the rock salt deforms mainly due to the destruction of crystalline grains and the emanation of gases with a large amount of acoustic emission. At higher pressures, the number of crystalline grains that collapse decreases, and it is assumed that rock salt deforms plastically, emitting fewer gases with less acoustic emission. The authors show that geogenic gas emission during deformation can provide additional clues containing information about the type and magnitude of deformation occurring in Earth's crust [23].

One of the tasks of modern geodynamics related to seismic activity and generation of ^{222}Rn volume activity anomalies is to identify the physical mechanisms of propagation and redistribution of energy of deformation processes in the geological medium. The block structure of Earth's crust and lithosphere significantly affects deformation, seismic, filtration, and other [24,25] processes. The correlation between seismic and radon activity is confirmed by numerous studies. It shows that seismicity and generation of RVA anomalies are controlled by some internal process and serve as its manifestation on Earth's surface.

As follows from the brief review above, the potential of joint radon and deformation monitoring for theoretical understanding of the mechanisms of radon concentration variations and their relation to tectonics and earthquake preparation, as well as the prediction of strong earthquakes, is beyond doubt.

Seismic activity in the modern world is one of the most dangerous threats to human life. Examples of such earthquakes that have occurred in the 21st century are the earthquakes in Turkey and Syria (6 February 2023, $M_w = 7.7$, which killed about 5000 people), the earthquake off the east coast of Honshu Island in Japan (11 March 2011, $M_w = 9.1$, which caused a catastrophic tsunami, the largest man-made disaster at a nuclear power plant, and killed about 20,000 people), the earthquake in the Indian Ocean on 26 December 2004 with a magnitude from $M_w = 9.1$ to $M_w = 9.3$. The focal point (hypocenter) was located 160 km to the west of Sumatra Island (Indonesia), at a depth of 30 km. The resulting tsunami, up to 10 m high, reached the coasts of Indonesia, Thailand, Sri Lanka, the south of India, and the east coast of Africa. As a result, it killed, according to various estimates, 225,000 to 300,000 people in 14 countries and affected about 2.2 million people. The earthquake and tsunami caused widespread destruction. The economic loss of Thailand was estimated at USD 5 billion, Indonesia USD 4.5 billion, India USD 4.5 billion, Sri Lanka USD 1.6 billion, and Maldives USD 1.3 billion. This is by no means a complete list of seismic catastrophes of the 21st century, but it already demonstrates the danger that Earth's depths conceal in themselves.

For the Kamchatka region, the problem of seismic activity has the highest priority, as the Kamchatka peninsula is one of the most earthquake-prone areas on Earth. The cities of Petropavlovsk-Kamchatsky, Yelizovo, and Vilyuchinsk are in the zone of impact of shaking of the highest category (up to 9 units), which once again proves the need to develop effective methods of seismic activity forecasting. A possible way to solve this problem is to create an effective forecasting system based on an in-depth understanding of the processes occurring in Earth's crust in preparation for a future earthquake source. One of the methods

of studying such processes is the monitoring of changes in the concentration of radon gas (^{222}Rn) in the subsurface, atmospheric air, and water [26]. Such changes may serve as precursor signals for the preparation of strong earthquakes. The study of ^{222}Rn variations in subsurface air helps to obtain information about geodynamic processes in the mountain massif and properties of the medium through which subsurface gases migrate. Long-term observations and their comparison with the seismic activity of the region make it possible to track changes in the character of geodynamic processes. This information can be used to search for precursor anomalies that may indicate the approach of a strong earthquake.

One of the uranium decay products is the noble gas ^{222}Rn. The decay of radon and its products occurs with the release of three types of radiation, by which its concentration can be measured. By diffusion and convection, radon is transported into the atmosphere. The Petropavlovsk-Kamchatsky geodynamic test site monitors ^{222}Rn at a network of sites. The network is created in such a way that the main attention is directed to the Avacha and Kronotsky Bays and the south of Kamchatka. The observation points are equipped with complexes for recording subsurface gases, primarily radon and hydrogen. The network has been operating in different configurations for more than 20 years. Based on the data obtained, including radon volumetric activity (RVA), two types of precursor anomalies were identified in the subsurface radon field for a number of earthquakes in the Avacha Gulf region. Type A anomalies are characterized by their in-phase manifestation at 3–5 points with a relative shift in time. The most common forms of these anomalies are bay-shaped and stepped, of different polarity. The precursor anomaly of type A was also registered for the deep (origin depth 177 km) Zhupanovskoe earthquake with $M_w = 7.2$ and for the earthquake on 3 April 2023 with $M_w = 6.9$. The possible cause of in-phase anomalies on the network of points of registration of subsurface gases is deformation processes such as a solitary "deformation wave", which can arise due to the quasi-viscous flow of geomaterial at the last stage of earthquake preparation. Type B precursor anomalies were registered, as a rule, in one point of the network, had a definite shape and were well distinguished on the general background.

Calculations performed by mathematical modeling methods have shown that the mechanism of such anomalies is associated with the injection of ^{222}Rn into the groundwater flow with complete transverse mixing under the influence of a deformation stress pulse [27]. Identification of signs of such processes in radon observation data is one of the urgent tasks of geophysics. Application of new experimental data of subsurface gas variations in comparison with data on the seismic activity of the region and investigation of ^{222}Rn migration processes with the help of the most modern methods of mathematical modeling in order to interpret anomalous effects preceding earthquakes is a new and actual research method in Earth sciences and, in particular, in the development of earthquake prediction methods.

An earthquake with magnitude $M_w = 7.0$ happened on 17 August 2024 at 19:10:26 (UTC) in the northern part of the Avacha Gulf, not far from the Shipunsky peninsula. This earthquake was later named Shipunsky in connection with the geographical location of the epicenter (52.931° N, 160.133° E). The epicentral distance to Petropavlovsk-Kamchatsky was 100 km, and the depth was 29 km, according to the National Earthquake Information Center (NEIC, U.S. Geological Survey). The intensity of shaking in Petropavlovsk-Kamchatsky was 6–7 points on the seismic intensity scale (SIS). Before this earthquake, a number of anomalous effects were registered in the subsurface radon field at the network of points [7] near Petropavlovsk-Kamchatsky. The data from radon monitoring before and after this earthquake were used in this work to estimate the changes in the radon flux density in the accumulation chamber.

The article has the following structure. Section 1 presents the introduction, literature review, and structure of the paper. Section 2 describes the methodology of the study, specifically the emanation method and the fractional derivative method. Section 3 briefly summarizes radon monitoring as the main method for obtaining the experimental RVA data used in the study. Section 4 describes the method for solving the direct problem for the hereditary α-model RVA. Section 5 formulates the inverse problem of recovering the values of several constant parameters λ_0 and α and describes the method of its solution. Section 6 introduces the concept of radon flux density and its relation to seismic activity and describes the method of radon flux density estimation. Section 7 presents the results of solving the inverse problems for λ_0 and α on the basis of different experimental RVA data, estimates the radon flux density on the basis of the reconstructed values of the parameters of the hereditary α-model RVA, and analyzes the sensitivity of the solution of the inverse problem. Section 8 summarizes the results of the study, formulates conclusions, and indicates further possible research direction.

2. Methodology

The research methodology in the article is based on the theory of the emanation method and the method of fractional derivatives. Let us consider them in more detail.

2.1. Emanation Method

The theory of the emanation method is based on the study of the process of mass transfer of radioactive gases (emanations) in the geological medium, as well as their flow into the surface layer of the atmosphere. The theory of the emanation method was developed for the purpose of searching for minerals (uranium ores) in the 1930s, but today, it is actively used to solve various problems, for example, related to the transfer of radionuclides the atmosphere [28], as well as in the tasks of prediction of strong earthquakes and mining strikes in deep mines [9,29,30]. The radioactive inert gas radon (^{222}Rn), which is the decay product of radium (^{226}Ra), is usually considered to be an emanation (Figure 1).

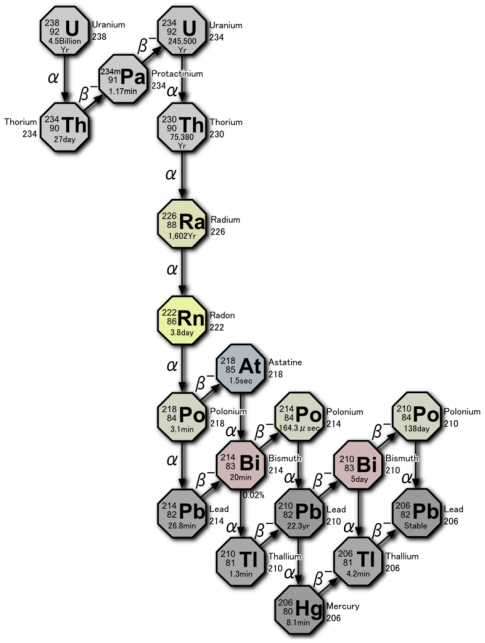

Figure 1. The radioactive series ^{238}U.

The research instrument in the scope of the theory of the emanation method is mathematical modeling. Mathematical modeling allows the development of various models of the radon-transport process in geo-medium. In diffusion-convective models, the mechanism of

radon transport occurs due to diffusion and convection (advection) [31]. In such models, radon transport is carried out along the spatial coordinate (stationary transport) as well as along time (non-stationary transport). In models of radon accumulation in chambers or confined spaces (mines), an important role is played by radioactive decay, radon entry, and exit through cracks and crevices [32]. In this article, we will consider the process of radon accumulation in a chamber according to the model [32]:

$$\frac{dA(t)}{dt} = S(t) - \left(A(t) - A_{Rn}^{atm}\right)\lambda_v(t) - \left(A(t) - A_{Rn}^{atm}\right)\lambda_{Rn}, \qquad A(t_0) = A_0, \tag{1}$$

where $A(t)$—radon volumetric activity (RVA), [Bq/m^3]; A_{Rn}^{atm}—RVA in outside air, [Bq/m^3]; $S(t)$—function responsible for the ^{222}Rn entering the chamber, [Bq/m^{3}s]; $\lambda_v(t)$—function responsible for the air exchange in the chamber, [s^{-1}]; $\lambda_{Rn} = 2.1 \cdot 10^{-6}$—radon decay constant, [s^{-1}]; $t \in [t_0, T]$—time of the process under consideration, [s]; t_0 and $T > 0$—initial and final time moments, [s];

Remark 1. *The model (1) may allow some simplifications. For example, the third term in the right-hand side of Equation (1) can be neglected because $\lambda_v(t) \gg \lambda_{Rn}$. This is due to the fact that even in a completely closed room, the values of the air exchange coefficient are an order of magnitude larger than the decay constant λ_{Rn}.*

Remark 2. *It is known that the transport of ^{222}Rn in the vertical direction can be caused by thermofluidic convection, turbulent effects due to changes in meteorological factors, diffusion due to the pressure gradient in Earth's crust, diffusion due to the concentration gradient of ^{222}Rn, and others [5]. Therefore, in the model (1), the value $S(t)$ describes simultaneously the convective $S^C(t)$ and diffusive $S^\Delta(t)$ mechanisms. Since there is no significant convective flow of subsurface air from the surface under the accumulation chamber, the term $S^C(t)$ can be ignored.*

Remark 3. *The modeled accumulation process ^{222}Rn can be considered stationary in the sense of inflow rate ^{222}Rn when the radon flux density (RFD) from the surface under the accumulation chamber is constant and when there are no sudden changes in the air exchange coefficient. Then the model parameters $\lambda_v(t) = \lambda_0$ and $S(t) = S$ are constant values, and the RVA will have an accumulative character with saturation yield: $A_{max} = S/\lambda_0$ [7]. Whence we obtain that $S = A_{max}\lambda_0$.*

Taking into account the remarks, the model (1) can be rewritten in a simplified form as follows:

$$\frac{dA(t)}{dt} = \lambda_0(A_{max} - A(t)), \qquad A(t_0) = A_0. \tag{2}$$

Let us rewrite Equation (2) for RVA in dimensionless form by normalizing by A_{max}:

$$\frac{d\bar{A}(t)}{dt} = \lambda_0(1 - \bar{A}(t)), \qquad \bar{A}(t_0) = \bar{A}_0, \quad \bar{A}(t) = \frac{A(t)}{A_{max}}, \quad \bar{A}_0 = \frac{A_0}{A_{max}}. \tag{3}$$

The solution of the model (3) is known, and it is of the form:

$$\bar{A}(t) = 1 - e^{-\lambda_0 t}(1 - \bar{A}_0), \qquad \bar{A}(t_0) = \bar{A}_0. \tag{4}$$

The solution (4) describes the accumulation process ^{222}Rn in the chamber and has an asymptotics $\bar{A}(t) \to 1$ at $t \to \infty$ (Figure 2).

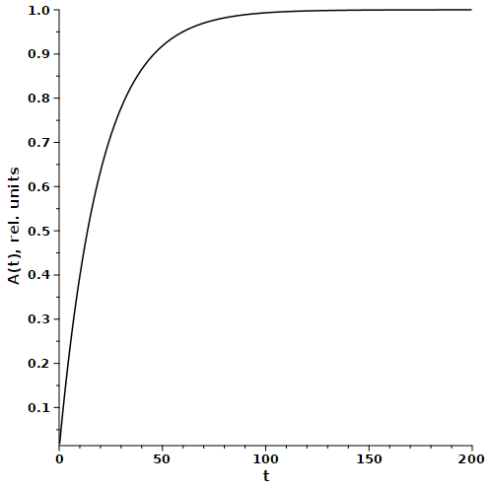

Figure 2. Solution graph (4).

The solution (4) is often applied to investigate the dynamics of RVA in an accumulation chamber when the geo- medium experiences a stress-strain state [7].

2.2. Fractional Derivative Method

The theory of the emanation method is based on its research on the fundamental principles of classical thermodynamics of non-reversible processes. Some of these principles, the principle of locality and the principle of local thermodynamic equilibrium, significantly impose limitations on the applications of this theory. This is because the process of mass transfer is nonlocal and occurs only in those systems that are not in a state of thermodynamic equilibrium. Therefore, there are often cases where radon has a high migration capacity [33,34]. It is impossible to explain this using only the diffusion mechanism. Diffusion does not give radon a chance to move to a distance of the order of more than ten meters before the decay of radon atoms reduces its concentration to a level indistinguishable from the background, even if its source is strong enough. Convection (advection) can also contribute to radon migration ability, but it can also be insignificant. Therefore, it is necessary to search for other mechanisms of transport or to study the properties of the geo-environment in which it occurs. For example, if the geosphere is considered to be a geosphere with a fractal structure [35]—very porous, heterogeneous media with complex pore space topology, then we can arrive at anomalous radon-transport processes (Levy flights), such as superdiffusion [36]. These processes are investigated in the framework of the concept of spatial non-locality.

Non-locality in time leads to less intensive processes, for example, subdiffusion. In this case, particles adhere to pore walls, which characterizes traps in which particles can stay for a long time. Time non-locality is related to the notion of heredity (memory) [37,38]. It means that particles, for some time, "remember" how they found their way into these traps.

Heredity effects occur in various systems, for example, in mechanical systems when describing visco-elastic-plastic media [39], in biological systems - when describing the viral propagation [40], in economic systems - when describing cycles and crises [41]. The mathematical apparatus of heredity research is based on the theory of integrodifferential equations developed by Italian mathematician Vito Volterra [42]. The peculiarity of integrodifferential equations is that the difference kernel in the integrand has certain properties (Volterra's hereditary principles) and is called a memory function.

Let us consider radon accumulation in the chamber, taking into account heredity. Let the dynamics of radon accumulation be described by the equation:

$$\int_0^t K(t-\tau)\dot{\bar{A}}(\tau)d\tau = F(\bar{A}(t), t), \tag{5}$$

where $K(t-\tau)$ is a memory function; $F(\bar{A}(t),t)$ is some function that is responsible for the mechanisms of radon accumulation; $\dot{\bar{A}}(\tau) = d\bar{A}(t)/dt$.

Equation (5) is integrodifferential and describes the hereditary process of radon accumulation in the chamber. If the memory function is chosen to be stepped, we can pass from the integrodifferential equation to the equation with fractional derivative, the apparatus of which is studied quite well [43,44]. The choice of the degree memory function is due to the fact that degree laws are often found in nature [45], for example, such laws as Gutenberg-Richter's law, Amory's law, etc. are known. In general, the memory function can be found by solving the corresponding inverse problem from experimental data.

Let us choose a memory function in the following form:

$$K(t) = \frac{1}{\Gamma(1-\alpha)\theta}\left(\frac{\theta}{t}\right)^{\alpha}, \tag{6}$$

where $\Gamma(.)$ is the Euler gamma function; θ is some characteristic time of the process [46], [s]; $0 < \alpha < 1$ is some parameter.

Substituting the ratio (6) into Equation (5), we obtain the following equation:

$$\frac{\theta^{\alpha-1}}{\Gamma(1-\alpha)}\int_0^t \frac{\dot{\bar{A}}(\tau)d\tau}{(t-\tau)^{\alpha}} = F(\bar{A}(t),t), \tag{7}$$

Given the definition of the fractional Gerasimov–Caputo derivative of order $0 < \alpha < 1$, which can be written as [47,48]:

$$\partial^{\alpha}_{0,t}\bar{A}(t) = \frac{1}{\Gamma(1-\alpha)}\int_0^t \frac{\dot{\bar{A}}(\tau)d\tau}{(t-\tau)^{\alpha}}. \tag{8}$$

As a result, we obtain the following model equation:

$$\theta^{\alpha-1}\partial^{\alpha}_{0,t}\bar{A}(t) = F(\bar{A}(t),t), \tag{9}$$

If we put in Equation (9) that $F(\bar{A}(t),t) = \lambda_0(1-\bar{A}(t))$, then we finally arrive at the equation:

$$\theta^{\alpha-1}\partial^{\alpha}_{0,t}A(\varphi) = \lambda_0(1-\bar{A}(t)), \tag{10}$$

For Equation (10), the local initial condition is true:

$$\bar{A}(t_0) = \bar{A}_0. \tag{11}$$

The problem (10), (11) admits an analytical solution in the form:

$$\bar{A}(t) = 1-(1-\bar{A}_0)E_{\alpha}\left(-\lambda_0\theta^{1-\alpha}t^{\alpha}\right), \tag{12}$$

where $E_{\alpha}\left(-\lambda_0\theta^{1-\alpha}t^{\alpha}\right) = \sum_{k=0}^{\infty}\frac{\left(-\lambda_0\theta^{\alpha-1}t^{\alpha}\right)^k}{\Gamma(1+\alpha k)}$—a special Mittag-Leffler function, whose properties are discussed in detail in [49].

Remark 4. *Please note that when $\alpha = 1$, the Mittag-Leffler function becomes an exponential, i.e., $E_1(-\lambda_0 t) = e^{-\lambda_0 t}$, and this leads us to the solution (4), which describes the accumulation of radon in the chamber without taking heredity into account.*

Remark 5. *It should be noted that the order of the fractional derivative may depend on time, which corresponds to the variable heritability [50,51]. In this case, the problem (10), (11) will be generalized, and its solution should be sought by numerical methods [52,53].*

In (Figure 3) in the Maple 2021 computer environment, the solution (12) was visualized as a function of different values of α at different times t, [h]. It should be noted that the calculated curves at small times at decreasing values of α indicate that the values of RVA are sharply increasing. Furthermore, starting from some time instant, the calculated curves regroup in the reverse order, forming steppe "tails", which indicates a slower exit to the asymptotics. The latter property is characteristic of nonlocal processes or processes with heredity.

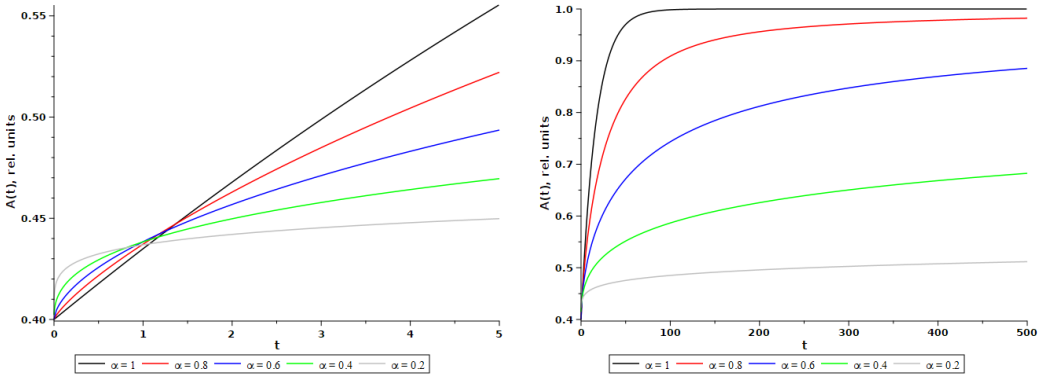

Figure 3. Calculated RVA curves plotted at $\theta = 1$ and different values of α: (**a**) $t \in [0.5]$; (**b**) $t \in [0.500]$.

Remark 6. *Please note that in the case of spatial non-locality for the diffusion-convective model of radon transport in the geosphere, the step tails in the calculated plots indicate an increase in the diffusion length of radon. The fractional derivative on the spatial coordinate has here the order of* $1 < \alpha < 2$, *which indicates superdiffusion. The (Figure 4) shows an example of calculations by the stationary diffusion-convective model of radon transport along the soil depth and their comparison with the experimental data, which were investigated in the article [54].*

In (Figure 4), it can be seen that the experimental curve is located closer to the curve $\alpha = 1.6$, compared to the curve for ordinary diffusion $\alpha = 2$, indicating the presence of fractal properties of the soil.

Based on the above, it can be assumed that the order of fractional derivative α is related to the permeability of the geo-environment. At the decrease of this parameter, the permeability of the medium increases, and it is easier for radon to penetrate through the ground into the accumulation chamber. Then, the mechanism of heredity is switched on, which gives a slowing down of radon output on saturation. The latter is characteristic of geo-mediated saturation.

In the present work, we use the above methodology to describe anomalous effects in the RVA time series that precede strong seismic events in Kamchatka.

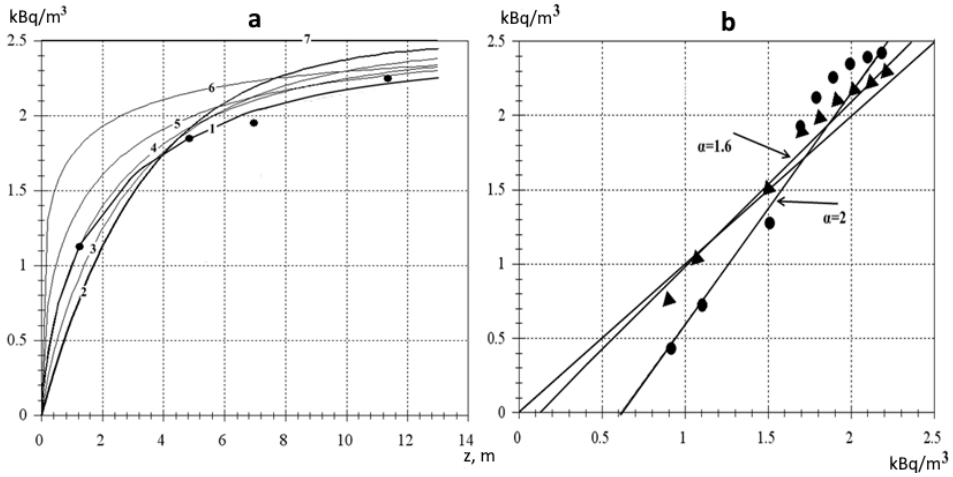

Figure 4. Radon concentration distribution curve by depth, drawn through the experimental points of the work [54], and the family of calculated curves of radon concentration in fractal medium with $A_\infty = 2.5$ [kBq/m^3] as a function of the parameter α (**a**): experimental curve (1), 2 (2), 1.8 (3), 1.6 (4), 1.4 (5), 1.2 (6), 1 (7). Correlation field between the RVA values of the experimental curve and the values of the calculated curves with $\alpha = 2$ and $\alpha = 1.6$ (**b**).

3. About Radon Monitoring

On the Kamchatka peninsula, a network of observation sites [55] has been deployed to monitor ^{222}Rn and additional environmental parameters (temperature, pressure, moisture, etc.) that can affect the resulting accumulation curve using accumulation chambers with gas-discharge counters. When planning the locations of subsurface gas-monitoring network stations in Kamchatka, special attention is paid to river valleys that run along crustal faults. These zones are characterized by increased permeability, which creates favorable conditions for subsurface gases to escape into the atmosphere, as described in the article [56].

Remark 7. *Analysis of RVA data and related parameters obtained during continuous monitoring is one of the methods of searching for earthquake precursors.*

This is due to the fact that RVA is affected by changes in the stress-strain state of the medium through which subsurface gas comes to the surface [57], so ^{222}Rn is considered a well-known and well-proven indicator of the processes occurring in such a medium [18,58]. Monitoring of ^{222}Rn as a method of searching for precursors of seismic events has proved itself in recent years [8], especially as a short-term precursor (up to 15 days) [59,60].

All points in the network are organized according to a common principle. The sensors are usually located in accumulation chambers (10 L galvanized buckets) in the aeration zone. When the equilibrium between ^{222}Rn and its decay products is reached in the accumulation chamber, the intensity of β-radiation increases, which increases the sensitivity of measurements. The insignificant convective component of subsurface air in the chamber was ensured by holes in the bottom of the bucket and loose packing of the pipe through which the detector was lowered into the chamber (Figure 5).

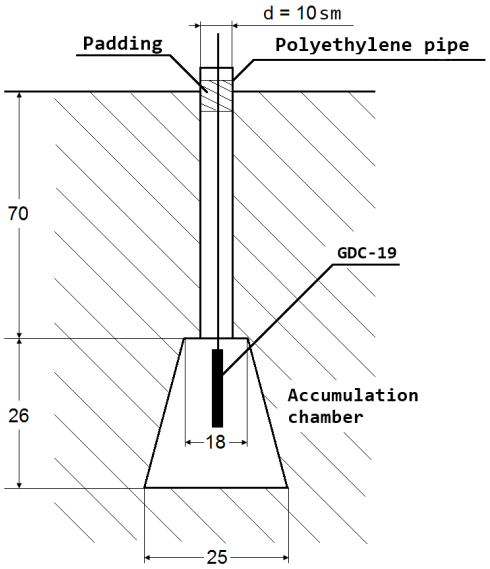

Figure 5. Scheme of placement of GDC-19 gas-discharge detectors for registration of β-radiation of radon decay products.

Gas-discharge counters are the most common detectors of β- and γ-radiation. The high sensitivity of counters allows the registration of single quanta of ionizing radiation, and the large output signal is easily registered by recalculation circuits. All this allows passive registration of ^{222}Rn in subsurface air by β-radiation of short-lived products of its decay with a high degree of reliability and rather simple metrology. Conversion from pulses to RVA is carried out by the empirical formula $A(t) = 9 \cdot M$ (Bq/m^3), where M is the number of pulses registered by β-radiation sensors per minute), obtained as a result of synchronous registration by certified radiometers RS-410F by femto-TECH (USA), RRA-01M-03 (Russia) and recorder with GDC-19 detector.

The data on (Figure 6) used in this work were obtained from the RVA sensor at the INSR point installed in the aeration zone of loose sediments at a depth of 3 m from the day surface [7]. On (Figure 6) shows the RVA and atmospheric pressure curves. On the RVA curve for estimation of radon flux density, the two least noisy areas were selected for exogenous impacts. In the second plot (Figure 6b), the abrupt release of RVA is associated with the arrival of a cyclone and a decrease in atmospheric pressure. To use these data for modeling purposes, the RVA data were removed at the specified site, and the skip was filled in using the Lubushin A.A. software package [61].

The figure shows that three days before the earthquake, there was a sharp decrease in RVA, and then followed by a new stage of accumulation. It is supposed that such behavior of RVA is connected with the last stage of development of the source of future earthquakes and is determined by the propagation of deformations in Earth's crust. Similar behavior of RVA curves was recorded before a number of strong earthquakes in southern Kamchatka and earlier [7].

Data from the KRMR point were provided by Makarov E.O., senior researcher of the laboratory of acoustic and radon monitoring of the Kamchatka branch of the Federal Research Center "Unified Geophysical Service of the Russian Academy of Sciences" Petropavlovsk-Kamchatsky, Russia. The work was supported by the Ministry of Education and Science of Russia (within the framework of the state task No. 075-00682-24) and with the use of data obtained at the unique scientific installation "Seismoinfrasound complex for monitoring of the Arctic cryolithozone and the complex of continuous seismic monitoring of the Russian Federation, neighboring territories and the world".

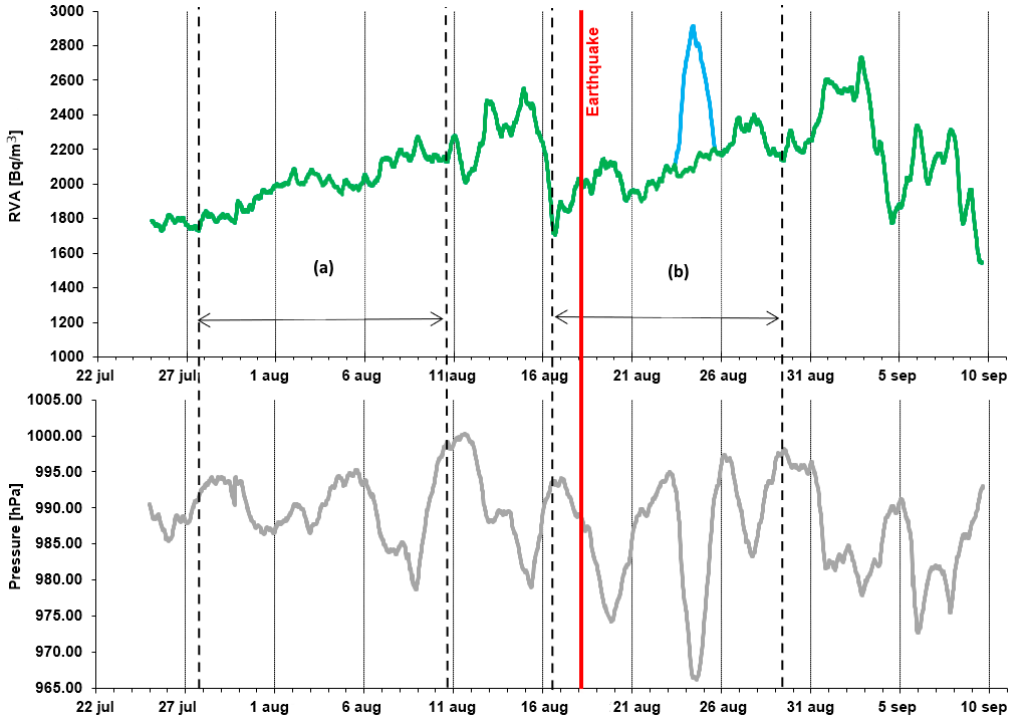

Figure 6. (green)—Experimental RVA data from the INSR observation site, in the temporal vicinity of the 50-day earthquake: (**a**)—RVA before earthquake, during 27 July 2024 (16:00)—10 August 2024 (15:30); (**b**)—RVA after earthquake, during 16 August 2024 (16:00)—29 August 2024 (15:30); (grey)—atmospheric pressure data at INSR point; (light blue)—excised section of the RVA due to the strong influence of reduced pressure; (red)—7.0 magnitude earthquake.

4. Direct Problem for the Hereditary α-Model RVA

The (1) and (3) equations use ODE, which significantly limits the flexibility of the ODE model. Therefore, the authors in [27,62] propose a modification of the (3) model consisting of replacing the first-order ordinary derivative by a fractional derivative of [43,44] of constant order.

Remark 8. *There are other definitions of the fractional order derivative. They can be found, for example, in scientific works [50,51,63]. However, the use of fractional Gerasimov–Caputo derivative (8) is the simplest and, at the same time, quite effective approach.*

A series of works by the authors of [27,52,62] is devoted to investigating issues related to mathematical modeling of RVA, where it is assumed that the parameter α describes the fractality of the [35] of the geo-medium and is related to its characteristics such as porosity, permeability, and fracturing.

To numerically solve the problem (10), we will use the previously developed nonlocal implicit finite-difference scheme (IFDS) [53] defined in a uniform grid domain:

$$\begin{gathered} h = T/N, \qquad \widehat{\Omega} = \{(t_i = ih) : 0 \le i < N\}, \qquad \widehat{\mathbb{A}} \in \widehat{\Omega}, \\ A(t) = A_i, \qquad 0 < A_i < 1. \end{gathered} \tag{13}$$

Definition 1. *Then, the difference direct problem:*

$$A_i = 1 - \frac{\widehat{\partial^{\alpha}_{0,ih}} A_i}{\lambda_0}, \qquad A_0 - const, \qquad 1 \le i < N, \qquad A(0) = A_0,$$
$$\widehat{\partial^{\alpha}_{0,ih}} A_i = \frac{h^{-\alpha}}{\Gamma(2-\alpha)} \sum_{j=0}^{i-1} \left((j+1)^{1-\alpha} - j^{1-\alpha} \right) (A_{i-j} - A_{i-j-1}). \tag{14}$$

is a Cauchy problem consisting of finding a discrete function A_i in the region $\widehat{\Omega}$ with known constants α and λ_0.

Remark 9. *IFDS scheme (14) and its generalized analogs have been tested in a number of tests and applied problems [53,64]. Then (14) is solved by the modified Newton method (MNM), and then the IFDS-based difference direct problem is unconditionally stable.*

Remark 10. *The hereditary α-model RVA (10) solved by the scheme (14) at the value $\alpha = 1$ will pass to the ODE model RVA (3), this is demonstrated in [52,64], which suggests that the generalization of (10) is correct.*

Next, in order to recover the values of the constant parameters λ_0 and α in the hereditary α-model RVA, from the known experimental RVA accumulation data before (Figure 7) and after (Figure 8) earthquake, the corresponding inverse problem [65,66] is formulated.

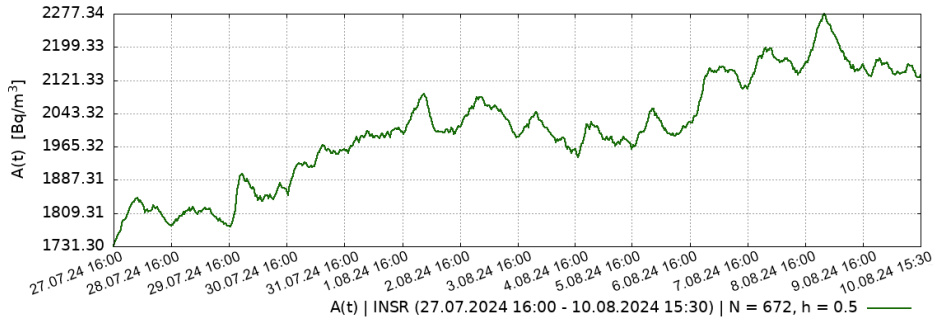

Figure 7. Experimental RVA data for 14 days, from the INSR observation point obtained before the earthquake during the period: 27 July 2024 (16:00)—10 August 2024 (15:30).

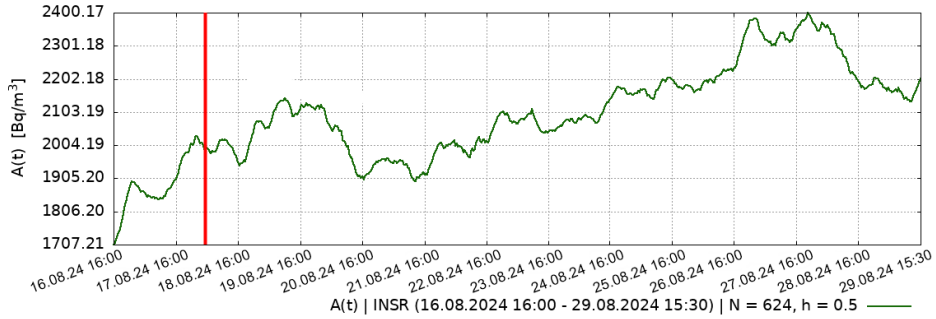

Figure 8. (green)—experimental RVA data for 13 days, from INSR observation point obtained after the earthquake (include earthquake) during the period: 16 August 2024 (16:00)—29 August 2024 (15:30); (red)—7.0 magnitude earthquake.

5. Inverse Problem on Parameters λ_0 and α for the Hereditary α-Model RVA

Previously, in [27,52,62] the parameters of models λ_0 and α were unknown and were selected by brute force based on some considerations about the process flow, which is a

time-consuming approach. The accuracy of the selection was evaluated by the maximum of R^2—the coefficient of determination and σ—the Pearson correlation coefficient with the maximum normalized experimental RVA data. This naturally leads to the search for solutions to automate the selection of optimal parameters.

Let $A_i \in \widehat{\mathbb{A}}$ (and correspondingly $A(t) \in \mathbb{A}$) be some function, but its solution depends on the set of parameters $\overrightarrow{X} = [X_0, \ldots, X_{K-1}]$, where $K = 2$, and $X_0 = \alpha$, $X_1 = \lambda_0$. Let the values of the discrete decision function $A_i \in \widehat{\mathbb{A}}$ are unknown, but additional information (experimental data of RVA) $A_i = \phi_i = \overrightarrow{\phi}$ on the solution of the direct Cauchy problem (14) for the hereditary α-model of RVA is known.

Definition 2. *Then the difference inverse problem for (14) is to restore the values* $\overrightarrow{X} = [X_0, X_1]$ *from the known* $A_i = \theta_i$ *experimental RVA data:*

$$\begin{gathered} A_i = 1 - \frac{\widehat{\partial^{X_0}_{0,ih} A_i}}{X_1}, \qquad A_i = \theta_i, \qquad 1 \le i < N, \\ \widehat{\partial^{X_0}_{0,ih} A_i} = \frac{h^{-X_0}}{\Gamma(2 - X_0)} \sum_{j=0}^{i-1} \Big((j+1)^{1-X_0} - j^{1-X_0} \Big) \left(A_{i-j} - A_{i-j-1} \right). \end{gathered} \tag{15}$$

To solve (15), we turn to the unconditional optimization theory [67]. For this purpose, it is necessary to minimize the bias functional:

$$\overrightarrow{\eta} = \overrightarrow{\theta} - \omega(\overrightarrow{X}), \qquad \min\left(\Psi\left(\overrightarrow{X}\right)\right) = \frac{1}{2} \sum_{i=0}^{N-1} \eta_i^2 = \frac{1}{2} \sum_{i=0}^{N-1} (\theta_i - \omega_i)^2, \tag{16}$$

where $\overrightarrow{\eta}$ is a bias vector of dimension $N > K$, and the vector $\omega(\overrightarrow{X}) = [\omega_0, \ldots, \omega_N]$ is a vector of model data, i.e., the solution of the difference direct problem (14) with respect to some approximation $\overrightarrow{X}$ obtained by solving the inverse problem.

The difference inverse problem is solved by a Newton-type unconditional optimization method [68], namely the Levenberg–Marquardt iterative method [69], represented as:

$$\Delta X = \left(-H^{-1}\right) \times \left(J^T \times \overrightarrow{\eta}\right), \qquad H = J^T \times J + \gamma E, \tag{17}$$

where

- ΔX—the optimal increment of $\overrightarrow{X}$ for the next iteration;
- E is a unit matrix of dimension $K \times K$;
- $J = J\left(\overrightarrow{X}\right)$—a Jacobi matrix of dimension $N \times K$ with elements calculated by the formula: $J_{i,k} = \frac{\partial \eta_i}{\partial X_k}, i = 0 \ldots N-1, k = 0 \ldots K-1$;
- the derivative $\frac{\partial \eta_i}{\partial X_k}$ is approximated by the difference operator $J_{i,k} = \frac{\eta_i^\delta - \eta_i}{\delta X_k}$, where δX—a given small increment of $\overrightarrow{X}$;
- γ is the regularization parameter of the method. If $\gamma \in \mathbb{R} > 0$ and the Hesse matrix H is positive definite, then ΔX is the direction of descent for the optimal step of the method;
- Start value: $\gamma^{(0)} = v \cdot \max\limits_i \left(diag\left(J\left(X^{(0)}\right)^T \times J\left(X^{(0)}\right) \right) \right)$, where v is a given starting constant.

Remark 11. *The solution of the inverse problem (15) by the Levenberg–Marquardt method (17), hereafter (IP-LB), is reduced to starting from the given constants* $X^{(0)}$, δX, v, *and* c*—constants for recalculating* γ *during the loop, by recomputing the solution of the difference direct problem (14) many times with approximations* $\overrightarrow{X}$ *obtained during the solution of the inverse problem, to compute*

the optimal values of $\overrightarrow{X}$*. More details on the algorithm for implementing the optimization of the vector* $\overrightarrow{X}$ *can be found in the article [70].*

The criterion for obtaining the optimal value is $\varepsilon \leq \Sigma$, where Σ is the given accuracy of IP-LB solution, $\varepsilon = \frac{1}{N}\sum_{i=0}^{N-1}\left[\eta_i^{\Lambda}\right]^2$—mean square error (MSE) between experimental and model RVA data.

All calculations related to the solution of direct and inverse problems by RVA models, as well as calculations on data processing, were performed in the PRPHMM 1.0 software package in MATLAB version R2023b for GNU/Linux Ubuntu Desktop 22.04. PRPHMM 1.0 is developed within the framework of the project "Modeling of dynamic processes in geospheres taking into account heredity" at the expense of the grant of the Russian Science Foundation № 22-11-00064 (head Parovik R.I.) implemented at the Institute of Cosmophysical Research and Radio Wave Propagation, Far East Branch of the Russian Academy of Sciences, Paratunka village, Russia.

6. Radon Flux Density and Its Relation to Seismic Activity

As the experience of long-term observations has shown, before strong earthquakes in southern Kamchatka, precursor anomalies are observed in the dynamics of RVA in the subsurface air, the amplitude of which is no more than 30% of the background [71]. To detect such precursor anomalies in the subsurface radon field in Kamchatka, as a rule, in-phase variations are searched at several registration points, and the peculiarities of the anomalies' occurrence are investigated using mathematical modeling methods. For example, in the paper [72] on the basis of a stationary mathematical model of diffusive-advective radon transport it is shown that in an inhomogeneous layered medium with increasing radon advection rate (v) the value of RVA increases proportionally, while the radon flux density (RFD) increases according to a quadratic dependence. In a homogeneous medium, when v increases by an order of magnitude, RFD also increases by an order of magnitude, while RVA increases insignificantly. The theoretical estimates were confirmed experimentally in [73], where it was shown that the dynamic characteristics of RVA in soil air are less sensitive to changes in the stress-strain state of the geo-environment in Kamchatka compared to RFD. As an example confirming this fact, we present the following graphs (Figure 9).

Before the earthquake with magnitude $M_w = 6.2$, which occurred on 24 August 2006 off the coast of southern Kamchatka at a distance of 190 km from the PRT point, there was observed an anomaly characterized by the increase of RVA values on the ground surface not more than 22% from the background (Figure 9a). At the same time, the calculated values of RFD and v increase almost one and a half times (RFD by 51%, Figure 9b). The radon flux density was calculated using the methodology proposed in the article [73].

It should be noted that using daily variations of atmospheric pressure as a probing signal of the ground state, the permeability coefficient was calculated, which during this period decreased almost 4 times: from $2.7 \cdot 10^{-13}$ to $6 \cdot 10^{-14}$ [m^2] [74]. The increase of RFD with a decreasing permeability coefficient testifies in favor of the fact that the mechanism of mass transfer in the considered period cannot be described within the framework of the classical diffusion-convection model. Therefore, it is possible that it is necessary to consider loose sediments as a porous medium with fractal properties.

The paper [75] presents data on RVA and RDF variations at one of the network sites before strong earthquakes in Kamchatka and concludes that the RFD parameter compared to RVA variations was more sensitive to changes in the stress-strain state of the medium before the deep Okhotomorsk earthquake with $M_w = 8.3$. In addition, in the records of radon flux density, a post-seismic effect associated with the change in ground permeability

after the 5-ball shaking caused by this earthquake in the vicinity of the observation point was detected, which was not manifested in the RVA variations.

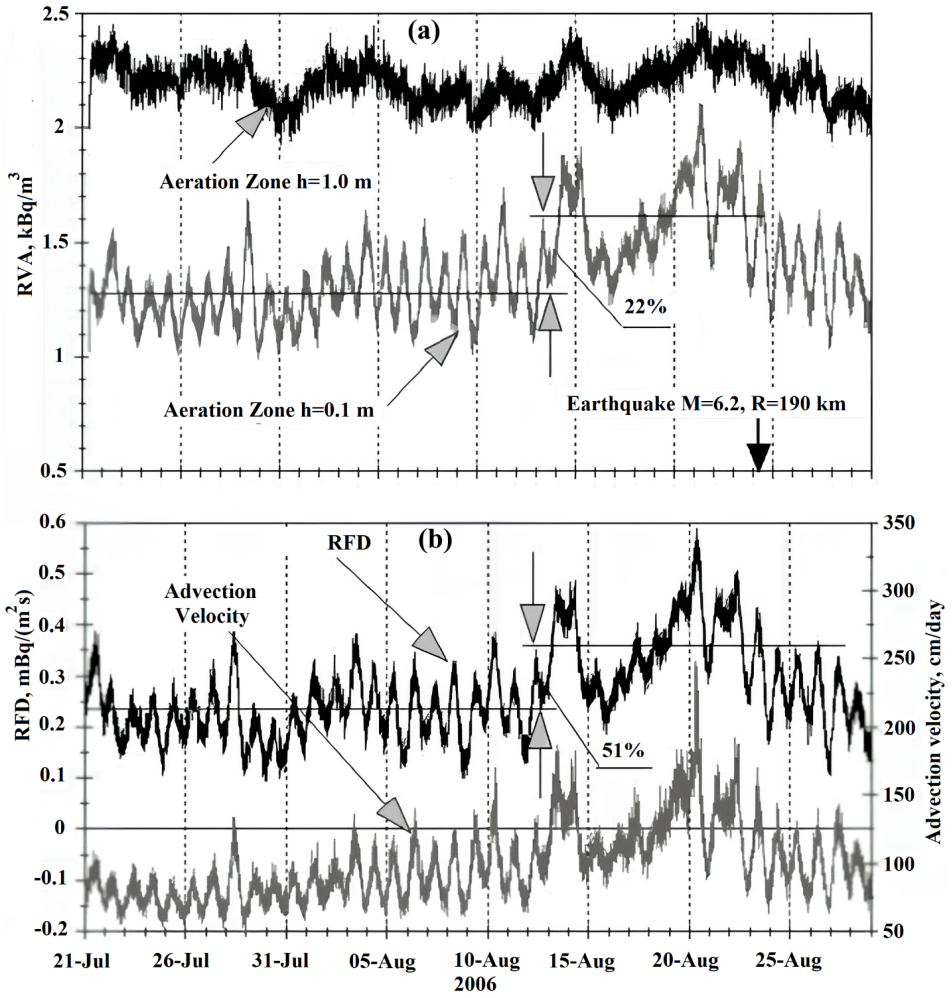

Figure 9. (**a**) RVA dynamics at the PRT point in the aeration zone at the depths of 0.1 and 1.0 [m] for the period 20 July–29 August 2006; (**b**) calculated RFD and v advection rate [74].

According to the [7] the arrival rate $^{222}\mathrm{Rn}$ is described by the relation: $S = q\Pi/V$. Then, to estimate RFD based on a model stationary in the sense of the arrival rate $^{222}\mathrm{Rn}$ (As observed in Section 2.2), it suffices to express:

$$q = \frac{A_{max}\lambda_0 V}{\Pi}, \tag{18}$$

where

- $S = A_{max}\lambda_0$—the arrival rate of $^{222}\mathrm{Rn}$ into the chamber, [Bq/m^{3}s];
- q—RFD from the surface under the accumulation chamber, [Bq/m^{2}s];
- Π—area of flow under the chamber (Figure 5), [m^2];
- V—volume of the accumulation chamber (Figure 5), [m^3].

Remark 12. *The parameters of the accumulation chamber at the INSR observation point (Figure 5) take the values:* $V = 0.01$, $\Pi = 0.05$.

It is also important to note that when working with experimental data, RVA is normalized to the maximum $A_{max} = 1$ [Rel.unit]. However, if we want to estimate RFD for the original RVA data, we should substitute the maximum un-normalized value in [Bq/m^3]

in place of A_{max}. However, the values of AER λ_0 before the earthquake (Figure 7) and after the earthquake (Figure 8) are unknown. However, by applying the method described above, it is possible to recover the values of the parameters α and λ_0 in the model (10) on the basis of experimental data on the variations of RVA in the accumulation chamber of the INSR point, and then to estimate the values of RFD before the earthquake and after the earthquake by (18).

Remark 13. *Algorithms realizing solutions of direct problems: by ODE model (4) and hereditary α-model (10) underlying the IP-LB algorithm, make calculations in "meter/hour" values. This is justified by the fact that the actual volume of the storage chamber (∼0.01 [m^3]) and the frequency of RVA registration (2 cycles/hour). However, for the convenience of perception, the other parameters of the models (4) and (10) were recorded according to the international system of SI units. Therefore, further on (Figures 10 and 11) the parameter values T, t, h in [h], and the recovered AER value $X_1 = \lambda_0$ in [h^{-1}]. Hence, to estimate the RFD (18), we need to divide λ_0 by* 3600 *to go to the scale [s^{-1}].*

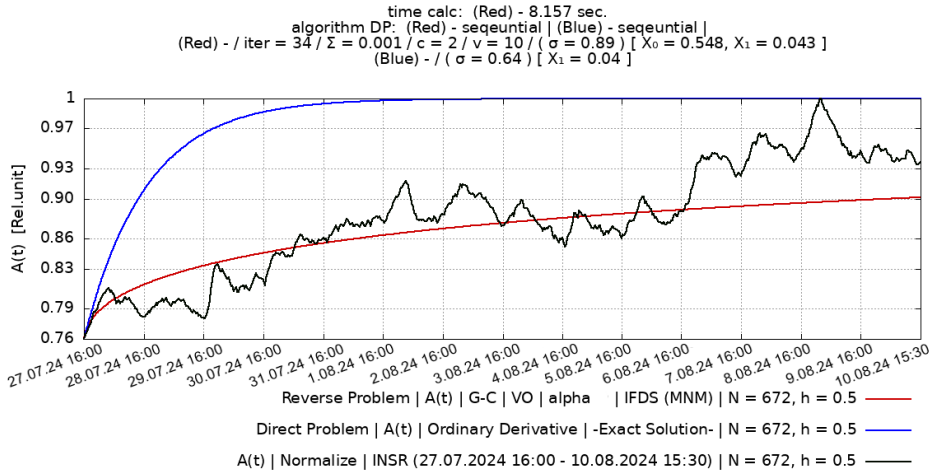

Figure 10. Modeling results based on RVA data before the earthquake.

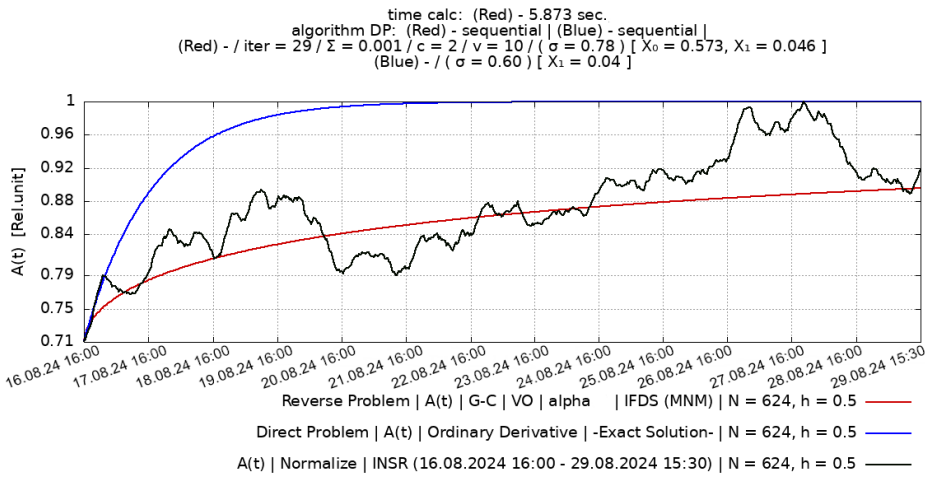

Figure 11. Modeling results based on RVA data after the earthquake.

Then for the camera in (Figure 5) RFD [Bq/m^2s] will be calculated by the formula:

$$q = \frac{A_{max}\lambda_0 V}{3600\Pi}, \tag{19}$$

7. Results of the Research

Visualization in this article was performed with the help of the FEVO 1.0 software package, developed also in the Gnuplot 6.0 scripting language for GNU/Linux Ubuntu Desktop 22.04. The FEVO 1.0 is developed within the framework of the project "Development of a software package for modeling and analysis of volumetric activity of radon as a precursor of strong earthquakes in Kamchatka" under the grant of the Russian Science Foundation № 23-71-01050 (supervised by D.A. Tverdyi) implemented at the Institute of Cosmophysical Research and Radio Wave Propagation, Far Eastern Branch of the Russian Academy of Sciences, Paratunka village, Russia.

Next, we will present the results of the IP-LB solution to recover the optimal values of $X_0 = \alpha$, $X_1 = \lambda_0$ of the stationary hereditary α RVA model (10) from the known experimental RVA data (Figures 7 and 8).

7.1. Results of Solving Inverse Problems

The results in (Figures 10 and 11) obtained with the following values of control parameters: $\left[X_0^{(0)}, \delta_0\right] = [0.05, 0.01]$ for the index α; and $\left[X_1^{(0)}, \delta_1\right] = [0.0025, 0.0005]$ for the coefficient λ_0. The values of the control parameters c, v, $\bar{\Sigma}$ described above for the IP-LB algorithm are shown in the figures.

The degree to which the model curves agree well with the experimental data was evaluated by σ—Pearson correlation coefficient with the processed experimental RVA data used for solving inverse problems. The key parameters characterizing the obtained results are reduced to "meter/second" according to the international system of SI units and are summarized in Table 1.

Table 1. Parameters of mathematical models: classical ODE (2), hereditary α-model RVA (10) solved by methods of inverse problems, as well as similarity coefficients of model curves and data.

INSR Dates Data Sampling	$\mathbf{A_{max}}$ [$\mathbf{Bq/m^3}$]	Set λ_0 for ODE [$\mathbf{s^{-1}}$]	Restore λ_0 for Heredity [$\mathbf{s^{-1}}$]	α for ODE	Restore α for Heredity	Correlation for ODE	Correlation for Heredity	RFD by ODE [$\mathbf{Bq/m^2s}$]	RFD by Heredity [$\mathbf{Bq/m^2s}$]
Before: 27 July 2024–10 August 2024	2277.34	$1.11 \cdot 10^{-5}$	$1.194 \cdot 10^{-5}$	1	0.548	64 %	89 %	$5.06 \cdot 10^{-3}$	$5.44 \cdot 10^{-3}$
After: 16 August 2024–29 August 2024	2400.17	$1.11 \cdot 10^{-5}$	$1.277 \cdot 10^{-5}$	1	0.573	60 %	78 %	$5.33 \cdot 10^{-3}$	$6.13 \cdot 10^{-3}$

Remark 14. *The recovery of λ_0 is strongly influenced by the choice of its control parameters in the IP-LB algorithm, i.e., $X_1^{(0)}$—the initial specified approximation and δ_1—the initial specified increment of $X_1^{(0)}$. It was observed that if the initial approximation and its increment are set $\pm 1\%$ of the estimate of the maximum value of the parameter to be recovered, the efficiency and accuracy of IP-LB will be the highest based on the estimates of the similarity coefficients for the described data samples.*

7.2. Sensitivity Analysis of the Solution

The first way to analyze the sensitivity of the solution to the inverse problem is to add a small perturbation $\epsilon = 10^{-4}$ to the right-hand side of Equation (15) as follows:

$$\begin{gathered} A_i = 1 - \frac{\widehat{\partial_{0,ih}^{X_0}} A_i}{X_1}, \qquad A_i = \phi_i, \qquad 1 \le i < N, \qquad A(0) = A_0, \\ \widehat{\partial_{0,ih}^{X_0}} A_i = \frac{h^{-X_0}}{\Gamma(2 - X_0)} \sum_{j=0}^{i-1} \left((j+1)^{1-X_0} - j^{1-X_0} \right) (A_{i-j} - A_{i-j-1}) + \epsilon. \end{gathered} \tag{20}$$

The second way to analyze the sensitivity of the solution to the inverse problem is to add a small perturbation $\epsilon = 10^{-4}$ to the initial condition (10) as follows:

$$A_i = 1 - \frac{\widehat{\partial^{X_0}_{0,ih}} A_i}{X_1}, \qquad A_i = \phi_i, \qquad 1 \le i < N, \qquad A(0) = A_0 + \epsilon,$$
$$\widehat{\partial^{X_0}_{0,ih}} A_i = \frac{h^{-X_0}}{\Gamma(2 - X_0)} \sum_{j=0}^{i-1} \left((j+1)^{1-X_0} - j^{1-X_0} \right) (A_{i-j} - A_{i-j-1}). \tag{21}$$

The following conclusions can be made from the results of sensitivity analysis (Table 2). The algorithm for solving the inverse problem produces the first solution calculated by it, which is closest to the optimal one. Furthermore, no matter how much we would not reduce the threshold of accuracy Σ when fixing the other control parameters, the solution algorithm "stuck", giving the same solution. Moreover, by introducing a small perturbation ϵ to the inverse problem (20) or (21), the algorithm also "stuck", but with some other solution (with different values of α and λ_0). This is very similar to the "local optimum trap", while the problem is to find the global optimum. Moreover, by introducing perturbations ϵ of different values (regardless of the order), the algorithm for solving the inverse problem converges to different points of the local optimum.

Table 2. Sensitivity analysis of the formulated inverse problem (15).

The Magnitude of Disturbance	INSR Dates Data Sampling	Not Disturbance Solve Inverse Problem (15)		With Disturbance Right Hence (20)		With Disturbance Initial Conditional (21)	
10^{-4}	27 July 2024–10 August 2024	$1.194 \cdot 10^{-5}$	0.548	$0.97 \cdot 10^{-5}$	0.526	$0.88 \cdot 10^{-5}$	0.556
10^{-4}	16 August 2024–29 August 2024	$1.277 \cdot 10^{-5}$	0.573	$0.94 \cdot 10^{-5}$	0.577	$1.30 \cdot 10^{-5}$	0.563
10^{-5}	27 July 2024–10 August 2024	$1.194 \cdot 10^{-5}$	0.548	$1.08 \cdot 10^{-5}$	0.57	$1.66 \cdot 10^{-5}$	0.525
10^{-5}	16 August 2024–29 August 2024	$1.277 \cdot 10^{-5}$	0.573	$1.44 \cdot 10^{-5}$	0.592	$1.19 \cdot 10^{-5}$	0.545
10^{-6}	27 July 2024–10 August 2024	$1.194 \cdot 10^{-5}$	0.548	$1.58 \cdot 10^{-5}$	0.55	$1.36 \cdot 10^{-5}$	0.539
10^{-6}	16 August 2024–29 August 2024	$1.277 \cdot 10^{-5}$	0.573	$1.36 \cdot 10^{-5}$	0.544	$1.0 \cdot 10^{-5}$	0.608

The obtained analysis results do not necessarily indicate that the solution of the posed inverse problem (15) is not the only one. However, it is clear that in the future it is necessary to apply more specialized methods to recover the parameters of the model equation. Nevertheless, a general trend in the recovered values can be seen, namely that α after the earthquake is larger than α before the earthquake when calculated with different values of the ϵ perturbation. No such dependence can be established for the parameter λ_0.

8. Conclusions

The scientific novelty of the presented paper consists of the fact that, for the first time, a hereditary mathematical model has been applied to estimate the change in radon flux density under changes in the stress-strain state of the medium under strong earthquake conditions. Moreover, RFD estimates before and after a strong earthquake were given for the first time.

The results presented in Table 1 show that according to the proposed hereditary α-model RVA, the radon flux density increased by 12.75%, while based on the ODE model RVA, the radon flux density estimate shows an increase of 5.39%. The obtained estimates agree with the existing RFD calculation theory.

The evaluations also showed that RFD increased after the earthquake, which is probably due to the impact of seismic waves on the ground in the area of the installation of the

storage chamber, as well as with the processes of relaxation of the geosphere arising after the seismic event. This impact led to a change in the permeability of rocks in the area of installation of the storage chamber and an increase in the total diffusive-convective flow of geo-gas. Post-seismic anomalous changes in RVA associated with the impact of seismic waves were recorded earlier in Kamchatka after the strong Zhupanovskoe earthquake (30 January 2016, $M_w = 7.2$).

The continuation of the study can be connected with the application of the described methodology of RFD estimation based on the results of parameter reconstruction of the hereditary α-model RVA, but already for experimental data on other earthquakes. It is also possible to complicate the model by adding a term to the equation to account for and compensate for the effects associated with the influence of atmospheric pressure and its variations on the RVA.

Also, the continuation of the research can be connected with the application of "neural networks" to restore the parameters of the hereditary α-model RVA in order to avoid falling into traps of local optimums (false attractors).

Author Contributions: Conceptualization, D.T., E.M., and R.P.; methodology, D.T. and E.M.; software, D.T.; validation, D.T., E.M., and R.P.; formal analysis, E.M. and R.P.; investigation, D.T. and E.M.; resources, D.T. and E.M.; data curation, E.M.; writing—original draft preparation, D.T. and E.M.; writing—review and editing, E.M. and R.P.; visualization, D.T.; supervision, R.P.; project administration, D.T.; funding acquisition, R.P. All authors have read and agreed to the published version of the manuscript.

Funding: The study was carried out with the financial support of the Russian Science Foundation (grants No. 22-11-00064 and No. 23-71-01050) and with the financial support of the Ministry of Science and Higher Education of the Russian Federation (075-00682-24) and the financial support of the State Assignment of IKIR FEB RAS (No. 124012300245-2).

Institutional Review Board Statement: Not applicable.

Informed Consent Statement: Not applicable.

Data Availability Statement: The original contributions presented in this study are included in the article. Further inquiries can be directed to the corresponding author.

Acknowledgments: The article is dedicated to the memory of Pavel Firstov, who made a significant contribution to the study of volcanic and seismic activity in Kamchatka. Under the leadership of P. Firstov, a radon monitoring network was organized in Kamchatka, and the theory of the emanation method was developed. The authors are grateful to P. Firstov for the valuable ideas and advice he gave when studying the topic of the article and are currently continuing his research.

Conflicts of Interest: The authors declare no conflicts of interest.

Abbreviations

The following abbreviations are used in this manuscript:

^{226}Ra	Radon
^{222}Rn	Radium
NEIC	National Earthquake Information Center
UTC	Coordinated Universal Time
SIS	Seismic Intensity Scale
RVA	Radon Volumetric Activity
GDC-19	Gas-Discharge Counter
RFD	Radon Flux Density
AER	Air Exchange Rate

ODE	Ordinary Differential Equation
FD	Fractional derivative
IFDS	Implicit Finite-Difference Scheme
MNM	Modified Newton's Method
IP-LB	Inverse Problem by method Levenberg–Marquardt
MSE	Mean Squared Error

References

1. Voitov, G.I. On the problems of hydrogen breath of the Earth. In *Degassing of the Earth: Geodynamics, Geofluids, Oil and Gas*; GEOS: Moscow, Russia, 2002; pp. 24–30. (In Russian)
2. Syvorotkin, V.L. *Deep Degassing of the Soil and Global Catastrophes*; Geoinformcenter LLC: Moscow, Russia, 2002; p. 250. (In Russian)
3. Zhang, W.; Lin, Y.Y. Preliminary study on the application of hydrogeochemistry of earthquake prediction. *Acta Seismologica* **1981**, *3*, 55–60.
4. Zubkov, S.I. Radon precursors of earthquakes. *Volcanol. Seismol.* **1981**, *6*, 74–105. (In Russian)
5. Dubinchuk, V.T. Radon as a precursor of earthquakes. In Proceedings of the Isotopic Geochemical Precursors of Earthquakes and Volcanic Eruption, Vienna, Austria, 9–12 September 1991; IAEA: Vienna, Austria, 1993; pp. 9–22.
6. Cicerone, R.D.; Ebel, J.E.; Britton, J. A systematic compilation of earthquake precursors. *Tectonophysics* **2009**, *476*, 371–396. [CrossRef]
7. Firstov, P.P.; Makarov, E.O. *Dynamics of Subsoil Radon in Kamchatka and Strong Earthquakes*; Vitus Bering Kamchatka State University: Petropavlovsk-Kamchatsky, Russia, 2018; p. 148. (In Russian)
8. Petraki, E.; Nikolopoulos, D.; Panagiotaras, D.; Cantzos, D.; Yannakopoulos, P.; Nomicos, C.; Stonham, J. Radon-222: A Potential Short-Term Earthquake Precursor. *Earth Sci. Clim. Chang.* **2015**, *6*, 1000282. [CrossRef]
9. Nikolopoulos, D.; Cantzos, D.; Alam, A.; Dimopoulos, S.; Petraki, E. Electromagnetic and Radon Earthquake Precursors. *Geosciences* **2024**, *14*, 271. [CrossRef]
10. Abduvaliev, A.K.; Voitov, G.I.; Rudakov, V.P. Radon precursor of some strong earthquakes in Central Asia. *Rep. USSR Acad. Sci.* **1986**, *291*, 924–927. (In Russian)
11. Teng, T.L. Some recent studies on groundwater radon content as an earthquake precursor. *J. Geophys. Res.* **1980**, *85*, 3089–3099. [CrossRef]
12. Yasuoka, Y.; Shinogi, M. Anomaly in atmospheric radon concentration: A possible precursor of the 1995 Kobe Japan, earthquake. *Health Phys.* **1997**, *72*, 759–761. [CrossRef] [PubMed]
13. Yasuoka, Y.; Igarashi, G.; Ishikawa, T.; Tokonami, S.; Shinogi, M. Evidence of precursor phenomena in the Kobe earthquake obtained from atmospheric radon concentration. *Appl. Geochem.* **2006**, *21*, 1064–1072. [CrossRef]
14. Chaudhuri, H.; Ghose, D.; Bhandari, R.K.; Sen, P.; Sinha, B. The enigma of helium. *Acta Geod. Geophys. Hung.* **2010**, *45*, 452–470. [CrossRef]
15. Hatanaka, H.; Kobayashi, Y.; Yasuoka, Y.; Nagahama, H.; Muto, J.; Omori, Y.; Suzuki, T.; Homma, Y.; Yamamoto, F.; Takahashi, K.; et al. Atmospheric radon concentration linked to crustal strain prior to and/or after earthquakes. In Proceedings of the 14th Workshop on Environmental Radioactivity, KEK, Tsukuba, Japan, 26–28 February 2013; pp. 379–385.
16. Zhou, S.; Tang, B.; Chen, R. SCADA-based Automatic Control System for Radon Chamber. In Proceedings of the 2009 International Conference on Electronic Computer Technology, Macau, China, 20–22 February 2009; IEEE: New York, NY, USA, 2009; pp. 448–451. [CrossRef]
17. Toutain, J.P.; Baubron, J.C. Gas geochemistry and seismotectonics: A review. *Tectonophysics* **1999**, *304*, 1–27. [CrossRef]
18. Neri, M.; Ferrera, E.; Giammanco, S.; Currenti, G.; Cirrincione, R.; Patanè, G.; Zanon, V. Soil radon measurements as a potential tracer of tectonic and volcanic activity. *Sci. Rep.* **2016**, *6*, 24581. [CrossRef] [PubMed]
19. Torres-González, P.; Moure-García, D.; Luengo-Oroz, N.; Villasante-Marcos, V.; Iribarren, I.; Blanco, M.J.; Soler, V.; Jiménez-Abizanda, A.; García-Fraga, J. Geochemical signals related to the 2011–2012 El Hierro submarine eruption. *J. Volcanol. Geotherm. Res.* **2019**, *381*, 32–43. [CrossRef]
20. Tuccimei, P.; Mollo, S.; Soligo, M.; Scarlato, P.; Castelluccio, M. Real-time setup to measure radon emission during rock deformation: Implications for geochemical surveillance. *Geosci. Instrum. Methods Data Syst.* **2015**, *4*, 111–119. [CrossRef]
21. Perna, A.F.N.; Paschuk, S.A.; Correa, J.N.; Narloch, D.C.; Barreto, R.C.; Claro, F.D.; Denyak, V. Exhalation rate of radon-222 from concrete and cement mortar. *Nukleonika* **2018**, *63*, 65–72. [CrossRef]
22. Cai, Z.-Q.; Li, X.-Y.; Lei, B.; Yuan, J.-F.; Hong, C.-S.; Wang, H. Laboratory Experimental Laws for the Radon Exhalation of Similar Uranium Samples with Low-Frequency Vibrations. *Sustainability* **2018**, *10*, 2937. [CrossRef]
23. Bauer, S.J.; Gardner, W.P.; Lee, H. Noble Gas Release from Bedded Rock Salt during Deformation. *Geofluids* **2019**, *2019*, 2871840. [CrossRef]

24. Kasahara, K. Migration of Crustal Deformation. *Dev. Geotecton.* **1979**, *13*, 329–341. [CrossRef]
25. Reuveni, Y.; Kedar, S.; Moore, A.; Webb, F. Analyzing slip events along the Cascadia margin using an improved subdaily GPS analysis strategy. *Geophys. J. Intern.* **2014**, *198*, 1269–1278. [CrossRef]
26. Rudakov, V.P. *Emanational Monitoring of Geoenvironments and Processes*; Science World: Moscow, Russia, 2009; p. 175. (In Russian)
27. Tverdyi, D.A.; Makarov, E.O.; Parovik, R.I. Hereditary Mathematical Model of the Dynamics of Radon Accumulation in the Accumulation Chamber. *Mathematics* **2023**, *11*, 850. [CrossRef]
28. Albdour, S.A.; Sharaf, O.Z.; Addad, Y. A critical review on the charging and transport dynamics of atmospheric radioactive aerosols: Fundamentals and advances. *Sci. Total Environ.* **2024**, *955*, 177130. [CrossRef]
29. Huang, P.; Lv, W.; Huang, R.; Luo, Q.; Yang, Y. Earthquake precursors: A review of key factors influencing radon concentration. *J. Environ. Radioact.* **2024**, *271*, 107310. [CrossRef]
30. Li, C.C.; Mikula, P.; Simser, B.; Hebblewhite, B.; Joughin, W.; Feng, X.; Xu, N. Discussions on rockburst and dynamic ground support in deep mines. *J. Rock Mech. Geotech. Eng.* **2019**, *11*, 1110–1118. [CrossRef]
31. Novikov, G.F. *Radiometric Intelligence*; Science: Leningrad, Russia, 1989; p. 406. (In Russian)
32. Vasilyev, A.V.; Zhukovsky, M.V. Determination of mechanisms and parameters which affect radon entry into a room. *J. Environ. Radioact.* **2013**, *124*, 185–190. [CrossRef] [PubMed]
33. Duddridge, G.A.; Grainger, P.; Durrance, E.M. Fault detection using soil gas geochemistry. *Q. J. Eng. Geol.* **1991**, *24*, 427–435. [CrossRef]
34. Kristiansson, K.; Malmqvist, L. Evidence for nondiffusive transport of 86Rn in the ground and a new physical model for the transport. *Geophysics* **1982**, *47*, 1444–1452. [CrossRef]
35. Mandelbrot, B.B. *The Fractal Geometry of Nature*; W.H. Freeman and Co.: New York, NY, USA, 1982; p. 468.
36. Evangelista, L.R.; Lenzi, E.K. Fractional Anomalous Diffusion. In *An Introduction to Anomalous Diffusion and Relaxation*; Springer: Berlin/Heidelberg, Germany, 2023; pp. 189–236. [CrossRef]
37. Parovik, R.I.; Shevtsov, B.M. Radon transfer processes in fractional structure medium. *Math. Model. Comput. Simul.* **2010**, *2*, 180–185. [CrossRef]
38. Uchaikin, V.V. *Fractional Derivatives for Physicists and Engineers. Vol. I. Background and Theory*; Springer: Berlin/Heidelberg, Germany, 2013; p. 373. [CrossRef]
39. Vlasov, V.V.; Rautian, N.A. A Study of Operator Models Arising in Problems of Hereditary Mechanics. *J. Math. Sci.* **2020**, *244*, 170–182. [CrossRef]
40. Ukaj, N.; Hellmich, C.; Scheiner, S. Aging Epidemiology: A Hereditary Mechanics–Inspired Approach to COVID-19 Fatality Rates. *J. Eng. Mech.* **2024**, *150*, 04024041. [CrossRef]
41. Makarov, D.V. The classical mathematical model of S.V. Dubovsky and some of its modifications for describing K-waves. *Bull. KRASEC Phys. Math. Sci.* **2024**, *46*, 52–69. [CrossRef]
42. Volterra, V. *Theory of Functionals and of Integral and Integro-Differential Equations*; Dover Publications: New York, NY, USA, 2005; p. 288.
43. Kilbas, A.A.; Srivastava, H.M.; Trujillo, J.J. *Theory and Applications of Fractional Differential Equations*, 1st ed.; Elsevier: Amsterdam, The Netherlands, 2006; p. 523.
44. Nakhushev, A.M. *Fractional Calculus and Its Application*; Fizmatlit: Moscow, Russia, 2003; p. 272. (In Russian)
45. Schroeder, M. *Fractals, Chaos, Power Laws: Minutes from an Infinite Paradise*; Dover Publications: Mineola, NY, USA, 2009; p. 448.
46. Rekhviashvili, S.S.; Pskhu, A.V. Fractional oscillator with exponential-power memory function. *Lett. ZTF* **2022**, *48*, 35–38. (In Russian) [CrossRef]
47. Novozhenova, O.G. Life And Science of Alexey Gerasimov, One of the Pioneers of Fractional Calculus in Soviet Union. *FCAA* **2017**, *20*, 790–809. [CrossRef]
48. Caputo, M.; Fabrizio, M. On the notion of fractional derivative and applications to the hysteresis phenomena. *Meccanica* **2017**, *52*, 3043–3052. [CrossRef]
49. Gorenflo, R.; Kilbas, A.A.; Mainardi, F.; Rogosin, S.V. *Mittag-Leffler Functions, Related Topics and Applications*; Springer: Berlin/Heidelberg, Germany, 2020; p. 540.
50. Patnaik, S.; Hollkamp, J.P.; Semperlotti, F. Applications of variable-order fractional operators: A review. *Proc. R. Soc. A* **2020**, *476*, 20190498. [CrossRef] [PubMed]
51. Sun, H.; Chang, A.; Zhang, Y.; Chen, W. A Review on Variable-Order Fractional Differential Equations: Mathematical Foundations, Physical Models, Numerical Methods and Applications. *FCAA* **2019**, *22*, 27–59. [CrossRef]
52. Tverdyi, D.A.; Makarov, E.O.; Parovik, R.I. Research of Stress-Strain State of Geo-Environment by Emanation Methods on the Example of alpha(t)-Model of Radon Transport. *Bull. KRASEC Phys. Math. Sci.* **2023**, *44*, 86–104. [CrossRef]
53. Tverdyi, D.A.; Parovik, R.I. Investigation of Finite-Difference Schemes for the Numerical Solution of a Fractional Nonlinear Equation. *Fractal Fract.* **2022**, *6*, 23. [CrossRef]

54. Spivak, A.A.; Sukhorukov, M.V.; Kharlamov, V.A. Peculiarities of radon 222Rn emanation with depth. *Dokl. Earth Sci.* **2008**, *421*, 823–826. [CrossRef]
55. Makarov, E.O.; Firstov, P.P.; Voloshin, V.N. Hardware complex for recording soil gas concentrations and searching for precursor anomalies before strong earthquakes in South Kamchatka. *Seism. Instrum.* **2013**, *49*, 46–52. [CrossRef]
56. Firstov, P.P.; Rudakov, V.P. Results of registration of subsoil radon in 1997–2000 at the Petropavlovsk-Kamchatsky geodynamic test site. *Volcanol. Seismol.* **2003**, *1*, 26–41. (In Russian)
57. Utkin, V.I.; Yurkov, A.K. Radon as a tracer of tectonic movements. *Russ. Geol. Geophys.* **2010**, *51*, 220–227. [CrossRef]
58. Barberio, M.D.; Gori, F.; Barbieri, M.; Billi, A.; Devoti, R.; Doglioni, C.; Petitta, M.; Riguzzi, F.; Rusi, S. Diurnal and Semidiurnal Cyclicity of Radon (222Rn) in Groundwater, Giardino Spring, Central Apennines, Italy. *Water* **2018**, *10*, 1276. [CrossRef]
59. İnan, S.; Akgül, T.; Seyis, C.; Saatçılar, R.; Baykut, S.; Ergintav, S.; Baş, M. Geochemical monitoring in the Marmara region (NW Turkey): A search for precursors of seismic activity. *J. Geophys. Res. Solid Earth* **2008**, *113*, 1–15. [CrossRef]
60. Biryulin, S.V.; Kozlova, I.A.; Yurkov, A.K. Investigation of informative value of volume radon activity in soil during both the stress build up and tectonic earthquakes in the South Kuril region. *Bull. KRASEC Earth Sci.* **2019**, *4*, 73–83. (In Russian) [CrossRef]
61. Lyubushin, A.A. *Analysing Data from Geophysical and Environmental Monitoring Systems*; Science: Moscow, Russia, 2007; p. 228. (In Russian)
62. Tverdyi, D.A.; Parovik, R.I.; Makarov, E.O.; Firstov, P.P. Research of the process of radon accumulation in the accumulating chamber taking into account the nonlinearity of its entrance. *E3S Web Conf.* **2020**, *196*, 02027. [CrossRef]
63. Coimbra, C.F.M. Mechanics with variable-order differential operators. *Ann. Der Phys.* **2003**, *12*, 692–703. [CrossRef]
64. Tverdyi, D.A.; Parovik, R.I. Application of the Fractional Riccati Equation for Mathematical Modeling of Dynamic Processes with Saturation and Memory Effect. *Fractal Fract.* **2022**, *6*, 163. [CrossRef]
65. Mueller, J.L.; Siltanen, S. *Linear and Nonlinear Inverse Problems with Practical Applications*; Society for Industrial and Applied Mathematics: Philadelphia, PA, USA, 2012; p. 351. [CrossRef]
66. Tarantola, A. *Inverse Problem Theory: Methods for Data Fitting and Model Parameter Estimation*; Elsevier Science Pub. Co.: Amsterdam, The Netherlands; New York, NY, USA, 1987; p. 613.
67. Dennis, J.E.; Robert, Jr.; Schnabel, B. *Numerical Methods for Unconstrained Optimization and Nonlinear Equations*; SIAM: Philadelphia, PA, USA, 1996; p. 394.
68. Gill, P.E.; Murray, W.; Wright, M.H. *Practical Optimization*; SIAM: Philadelphia, PA, USA, 2019; p. 421.
69. More, J.J. The Levenberg-Marquardt algorithm: Implementation and theory. In *Numerical Analysis*; Watson, G.A., Ed.; Lecture Notes in Mathematics; Springer: Berlin/Heidelberg, Germany, 1978; Volume 630, pp. 105–116. [CrossRef]
70. Tverdyi, D.A.; Parovik, R.I. The optimization problem for determining the functional dependence of the variable order of the fractional derivative of the Gerasimov-Caputo type. *Bull. KRASEC Phys. Math. Sci.* **2024**, *47*, 35–57. (In Russian) [CrossRef]
71. Firstov, P.P.; Mandrikova, O.V.; Filippov, Y.A. Anomalies in the dynamics of soil radon at the Petropavlovsk-Kamchatsky Geodynamic Test Site in 1997–2001: Precursors of strong earthquakes. *Dokl. Earth Sci.* **2003**, *389*, 462–465.
72. Yakovleva, V.S.; Karataev, V.D. Radon flux density at the Earth's surface as a possible indicator of the stress and strain state of the geological environment. *J. Volcanolog. Seismol.* **2007**, *1*, 67–70. [CrossRef]
73. Parovik, R.I.; Firstov, P.P. The Algorithm of Calculation of Density of a Stream of Radon (^{222}Rn) from the Surface of the Ground. *Vestn. Tomsk. Gos. Univ. Mat. Mekh.* **2008**, *3*, 96–101.
74. Firstov, P.P.; Ponomarev, E.A.; Cherneva, N.V.; Buzevich, A.V.; Malysheva, O.P. On the effects of air pressure variations on radon exhalation into the atmosphere. *J. Volcanolog. Seismol.* **2007**, *1*, 397–404. [CrossRef]
75. Firstov, P.P.; Makarov, E.O.; Glukhova, I.P. Parameter Variations in the Subsoil Radon Field at the Paratunka Station of the Petropavlovsk-Kamchatsky Geodynamic Test Site in 2011–2016. *Seism. Instrum.* **2018**, *54*, 121–133. [CrossRef]